MECHANICAL PERFORMANCE OF CARBON-FIBRE- AND GLASS-FIBRE-REINFORCED EPOXY I-BEAMS: I. MECHANICAL BEHAVIOUR

M. D. Gilchrist,[a] A. J. Kinloch,[b] F. L. Matthews[c] & S. O. Osiyemi[b]

[a] *Mechanical Engineering Department, University College Dublin, Belfield, Dublin 4, Rupublic of Ireland*
[b] *Mechanical Engineering Department, Imperial College, Exhibition Road, London SW7 2BX, UK*
[c] *Centre for Composite Materials, Imperial College, Prince Consort Road, London SW7 2BY, UK*

Abstract

This paper is the first in a series which detail the mechanical behaviour, finite element predictions and fractographic observations of the failure of composite I-beams. Experimental investigations into the behaviour under static load of both unnotched and web- and flange-notched continuously reinforced carbon-fibre/epoxy and glass-fibre/epoxy I-beams are discussed. A four-point flexural configuration is used. The global static response and ultimate failure are described in terms of strains, compliance, buckling and final fracture. A mode of buckling that is antisymmetric across the width of the compressive flange is observed prior to failure in all cases. Failure of the unnotched I-beams is concentrated around a buckle on the compressive flange whilst failure of the notched I-beams initiates from a shear-loaded circular cutout within the web. Buckling of the unnotched beams occurs at loads that are approximately 50% of the failure loads. Failure of the notched beams occurs at loads that are approximately 75% of the failure loads of the unnotched beams. Buckling and failure of the glass/epoxy beams occur at loads that are approximately 75% of the corresponding loads in the carbon/epoxy beams.

Keywords: I-beam, fracture, buckling, cutout, hole, notch, carbon and glass fibre, epoxy, static load, four-point bending, flexure, strength, stiffness, compliance, failure

NOTATION

a	Distance support to loading points in test setup (250 mm)
A	Cross-sectional area of web
b	Flange free half-width (33 mm)
E	Young's modulus
EI	Flexural rigidity
G	Shear modulus
GJ	Torsional stiffness
I	Moment of inertia
J	Polar moment of inertia
K	Buckling coefficient
l	Length
L	Distance between central loading points in test setup (500 mm)
P	Load applied by machine actuator
t	Flange thickness (3 mm)
X	Strength
y	Distance from the neutral axis of the I-beam to the centre of the flange (61 mm)
δ	Displacement (measured at actuator/yoke or midlength of beam)
ν	Poisson's ratio

Subscripts

c	Critical
I	Mode I (opening or tensile)
L	Longitudinal (laminate property dependent upon stacking sequence)
L_{ten}	Longitudinal tensile
max	Maximum
T	Transverse (laminate property dependent upon stacking sequence)
T_{ten}	Transverse tensile
yoke	Measured at loading yoke (= actuator)
11	Longitudinal (unidirectional ply property)
22	Transverse (unidirectional ply property)

1 INTRODUCTION

I-section components are typically used as structural support members in the wings of aircraft, tailcones of helicopters, cores of rotor blades[1] or in civil engineering structures. Depending on what is

connected to an I-beam, there will be greater or lesser amounts of tension or compression on the flanges and shear in the web of the beam. There may well be some degree of torsion along the length of the beam, although the low torsional rigidity of I-sections makes it desirable to minimise this in practical situations. The flanges may have an array of bolt holes for the attachment of panels or skins whilst the web region may have access holes for ducting or cables. Both types of hole will act as stress concentrators from where damage and component failure may initiate. Whilst laboratory tests attempt to simulate actual operating conditions, many approximations and assumptions are often made both for convenience and in order to obtain results of more widespread and general applicability. For example, within shear tests,[2,3] cantilever tests,[4] three-point bendings[5–8] and four-point flexure,[9–12] the precise manner in which load is introduced into the structural component may not represent truly the load distribution throughout a beam under operating conditions. In such experimental work it is often necessary to provide flange stiffeners to prevent buckling, or local reinforcement under the loading point to avoid premature failure in the loading regions, particularly when loading attachments may be drilled through the web of a beam and consequently act as damage initiation sites. Similarly, the boundary conditions at the loading points[13–17] will also influence the structural response of an I-beam. Clearly the mechanical behaviour of any beam will depend greatly on the various holes, attachments and stiffening stringers, as well as on the particular manufacturing process and any production defects[5,7,18–22] which are likely to be associated with the component.

Structural instability occurs when the stresses are such that the equilibrium of the member changes from stable to neutral. This critical load level is associated with compressive or shear stresses acting upon the member and is evidenced by the onset of buckling which, if load levels are increased, is eventually followed by structural failure of the component. The instability of both closed and open structural sections depends on EI, GJ, the position of the shear centre with respect to the centre of gravity, the cross-sectional symmetry and the material characteristics of the particular component. For practical design purposes it is important to predict, for a known set of external loads, the consequent deformation and distribution of internal stresses which are dependent upon these various parameters. Within I-section beams, lateral torsional buckling, warping, local flange buckling due to compression and local web buckling due to shear are the four forms of structural instability which can possibly occur.[13,23] It is worth noting that second and higher order modes of buckling can occur at higher loading levels prior to catastrophic failure.

For example, the static failure of E-glass/epoxy composite box beams, tested under four-point flexure,[9,10] has been found to be localised on the compressive face of the beam, close to one of the loading points. Carbon-fibre/thermoplastic-matrix composite I-beams tested under three-point bending failed in the compression flange[8] although this manner of failure was suppressed in further tests by using adhesively-bonded carbon-fibre/epoxy composite reinforcement caps. Failure in these instances then occurred due to either shear of the web or delamination of the tensile or compressive flange caps.

A complete fractographic analysis of the fracture surfaces can identify the origins and subsequent fracture directions within a structural component.[5,7,18–21] To describe properly the fractographic features observed within the beams of the present study is beyond the scope of this particular article and shall be dealt with elsewhere.[24] Purslow[5] has examined the static failure of a carbon-fibre/epoxy I-beam under three-point flexure where load was introduced to the web of the beam by drilling straight through reinforcement pads and the web of the beam. Delamination mostly occurred in the compression cap of the I-beam as a consequence of interlaminar shear between the 0°/45° and +45°/−45° plies. The most significant features were evident in the matrix material rather than the fibres, with shear cusps (hackles) indicating the local loading direction. Critical failure occurred in the compression cap as a result of an in-plane shear stress concentration which was located at the termination of the ±45° plies which coincided closely with the boundaries of one of the central reinforcement pads.

The present paper outlines the mechanical response of unnotched carbon-fibre/epoxy and glass-fibre/epoxy I-beams, as well as the behaviour of identical beams which contain a series of holes in the web and flange regions. The method of construction, from continuous prepreg tape, is outlined together with the four-point flexural testing arrangement. The physical response, buckling and progression of damage to failure of the beams are discussed in terms of measured strains, loads, deflections and compliance changes.

2 EXPERIMENTAL

The I-beams, of length 1200 mm, web depth 125 mm, flange width 75 mm and thickness 3 mm, were manufactured by co-curing two preformed C-channels of 12 plies together with two rectangular strips or caps, also of 12 plies, resulting in web and flange thicknesses of 3 mm. Figure 1 details the general method of beam manufacture. A 3 mm radius fillet exists at the corners of the web/flange region in order to avoid the excessively high stresses which could be

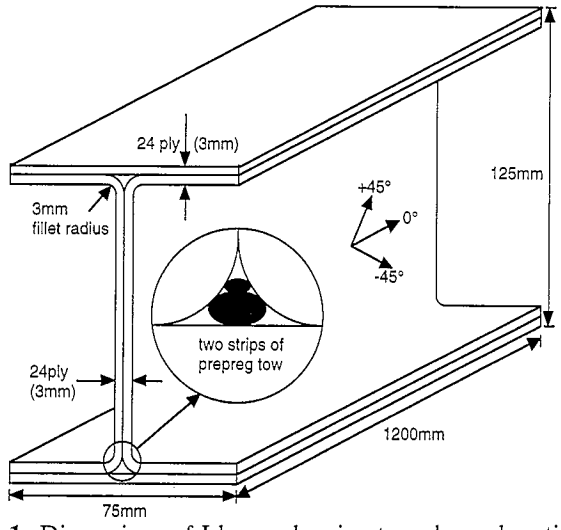

Fig. 1. Dimensions of I-beam showing two channel sections, two flange caps and strips of wound prepreg tow. The 24-ply stacking sequence is $(-45°/0°/45°)_{2s}(45°/0°/-45°)_{2s}$.

associated with a sharp corner. Two ropes (tows) of the same material are used to fill the triangular void which exists between the flange and web areas behind the fillet radii on the C-sections. The rope is formed from strips of spirally wound prepreg which are allowed to relax unconstrained prior to being implanted into the fillet region. A unidirectional process control laminate is laid up from 16 plies of the same material and cured together with the I-beam. This control laminate is subsequently used to verify certain mechanical properties after the curing and post-curing cycles have been completed; these cycles are in accordance with the manufacturer's instructions.

When manufacturing the I-beams, the preformed channel sections and the two flange caps were contained within a mould at autoclave conditions that were in accordance with the curing procedures of the material supplier. However, in order to counteract the effects of thermal strains (resulting from the different thermal expansion coefficients of the resin and the fibre and the anisotropic nature of the prepreg layup), a slight taper of 1–2° was machined on the channel of the mould. This ensured that when springback of the flanges occurred, the web/flange angle would be 90°. In some instances, the I-beams were warped along their length. This may have been due to the antisymmetric and multidirectional stacking sequence that had been used. This warpage was removed by constraining the beam during the post-curing cycle.

The layup, which has been used in the web and flanges of all the I-beams of this research, contains a balanced but antisymmetric combination of +45, 0° and −45° plies, where the 0° direction is defined to be along the axis of the beam. The 0° plies have been incorporated into the design primarily for sustaining the tensile and compressive loadings which exist within the beam flanges, whilst the +45° and −45° layers bear the shear loads occurring within the web region. Commercially available software[25] was used to design the beam stacking sequence such that there was the minimum number of coupling terms in the laminate stiffness matrix as well as the lowest possible interface moment, i.e. the τ_{zx} and σ_z stresses through the I-beam thickness were minimised. More specifically, the 24-ply stacking sequence is of the general form $[(L), (-L)]$ where (L) is a balanced, symmetric, multidirectional sublaminate, and $(-L)$ is a modified version of (L) in which the angular orientation of the off-axis plies is reversed. This stacking sequence ensured that there was zero bend–twist coupling. A further detail of the particular layup used was that a certain number of the +45°/−45° plies are interspersed with 0° plies providing sublaminates of the form $(+45°/0°/-45°)$ or $(-45°/0°/+45°)$. This has the effect of reducing interlaminar stresses within the laminate. The actual stacking sequence which was used is $(-45°/0°/+45°)_{2s}(+45°/0°/-45°)_{2s}$, i.e.

$$-45°/0°/45°/-45°/0°/45°/45°/0°/$$
$$-45°/45°/0°/-45°/45°/0°/-45°/45°/0°/$$
$$-45°/-45°/0°/45°/-45°/0°/45°$$

The mechanical properties of the Ciba Geigy carbon/epoxy, T300H/914, and glass/epoxy, E-glass/914, material systems were measured in accordance with the CRAG guidelines[26] and are given in Table 1. This table details both the unidirectional properties as well as those corresponding to the multidirectional stacking sequence that was used to manufacture the I-beams.

Common methods of loading I-beams for failure studies are either through the web or both flanges, or indeed through both simultaneously. When loading through the beam flange, line or surface rollers are often used, although these induce severe local stresses with damage and ultimate failure invariably emanating from under and around the loading nose. One restriction associated with flange loadings is that reversed loads are not possible unless some yoking mechanism is attached to both flanges of the beam. Similarly with web loading arrangements it is common to load directly through the web after drilling a loading point through the neutral axis of the beam. Such an operation obviously destroys the integrity of the beam and critical damage can often be traced back to this region. Consequently, it is usual to reinforce beams locally at the points of load introduction in order to avoid, or at least minimise, any damage which can occur in such regions. It is most important that both flange and web loading arrangements are carefully aligned in order that symmetry is maintained and that off-axis loads do not arise.

Within the present investigations, I-beams are tested under four-point flexure using either a load or a

Table 1. Measured mechanical properties of unidirectional and multidirectional carbon/epoxy (T300H/914) and glass/epoxy (E-glass/914) materials

Property	T300/914		E-glass/914	
	Unidirectional	Multidirectional	Unidirectional	Multidirectional
E_{11} (GPa)	134·75	54·75	45·37	26·68
E_{22} (GPa)	8·24	21·98	15·20	16·94
ν_{12}	0·325	0·704	0·289	0·477
ν_{21}	0·012	0·287	0·074	0·291
$X_{L_{ten}}$ (MPa)	1563·00	534·20	1049·00	432·77
$X_{T_{ten}}$ (MPa)	44·76	277·12	46·48	220·45
G_{12} (GPa)	Not measured	—	6·03	—

The stacking sequence used for the multidirectional laminates was the same as that used to manufacture the I-beams, namely $(-45°/0°/45°)_{2s}(45°/0°/-45°)_{2s}$. Note that no shear modulus was measured for the multidirectional stacking sequence: this is in agreement with the CRAG guidelines.[26]

displacement mode of control. A single actuator of a 250 kN servohydraulic (ESH Ltd) biaxial fatigue machine has been used to test these components and the various fixtures have been designed to withstand 200 kN fatigue loadings for up to 20 million cycles. Static tests have been under displacement control, whilst fatigue tests[11,12] have been carried out under load control. The loading is introduced to the beam simultaneously through the web and flange regions as detailed in Fig. 2. Eight loading pads are adhesively bonded to the I-beam (four on either side) with two yokes being used to transfer the actuator load to the four central loading pads and thence to the beam. The loading pads have a bonding surface of 117 mm × 117 mm that is bonded to the web face and of 20 mm × 117 mm to the underside of the flanges. This arrangement assumes a nominal bondline thickness of 1 mm between the loading pads and an I-beam. Four links are used to attach the outer loading points to the bed of the machine. This manner of loading avoids damaging the integrity of the beam and also obviates the need to post-cure composite reinforcements to the loading regions of the beam, which would of course alter the configuration of the component being tested. The loading pads also act as partial flange stiffeners such that the greatest length of unstiffened flange is between the two pairs of central loading pads (i.e. 383 mm). This has the effect of increasing the buckling load above that which would be associated with a loading arrangement that was solely through the I-beam web regions.

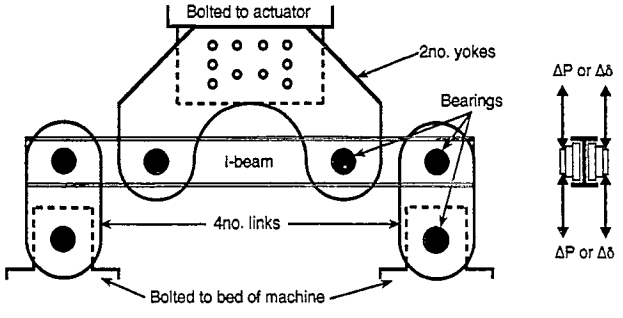

Fig. 2. Schematic diagram of the four-point flexure loading arrangement used for static and fatigue tests of I-beams.

During some initial I-beam fatigue tests, it was found that, rather than inducing damage within the structural component, the adhesive which had been used to bond the loading pads to the I-beams had fractured. For this reason, all subsequent loading pads were bonded using a high temperature cure-toughened adhesive of higher shear and peel strength, which performed satisfactorily throughout all the tests. The bonding of the hardened steel (EN24 grade) loading pads was done in one single operation using a steel jig to space the loading pads appropriately along the length of the beams.

Surface strains from gauges at a range of web and flange positions on the beams were recorded by using a 64-channel data acquisition system which operated on a keypress sequence. Typically, shear rosettes were situated along the neutral axis of the I-beam in the web regions between the loading pads. Strain gauges were located along both the tensile and compressive flanges, between the two central pairs of loading pads, where the flange stresses were maximum. Gauges were used on both the top and bottom faces of the flanges in order to detect any buckling. A dial gauge was also used to record the maximum beam deflections, i.e. at the centrespan, until creaking noises, which may have corresponded to the fracture of fibres, were heard. A linear variable differential transducer (LVDT) was also used to monitor these deflections from zero load until the onset of compressive flange buckling. However, it was principally readings of applied actuator load and displacement, obtained directly from the machine, which were used. It is important to remember that actuator displacement refers to that at the central load

attachment points, i.e. the yokes, and not to the displacement at the centrepoint of the beam. Classical beam theory can, however, be used to relate these yoke displacements to the maximum centre span displacements, i.e. $\delta_{max} = (11/8)\delta_{yoke}$.

Whilst two beams were tested statically in the virgin unnotched state, two identical beams had notches machined in the web and flange regions as shown in Fig. 3. Preliminary studies compared the effect of circular and diamond-shaped cutouts in the web region of a carbon/epoxy I-beam. It was found that a circular hole, of diameter equal to the maximum dimension of the diamond cutout, resulted in an I-beam which was weaker under shear. It is of interest to note that Ahlstrom and Bäcklund[27] predicted numerically that circular holes are weaker than rectangular or diamond cutouts when loaded in shear. Therefore, for the present studies, two circular holes of diameter 46 and 60 mm were cut, using a diamond-coated circular saw, in the two web regions between the sets of outer loading pads where the shear is constant and a maximum. The holes were centrally located in the web regions between the loading pads along the neutral axis of the beam. The diameters of these holes were selected such that the maximum hole dimension was 40 and 50% of the internal web depth, respectively. These web cutouts are representative of lightening holes or access ports within an I-section component, although it is worth noting that in common engineering practice it is unlikely that any web notch would exceed about 40% of the internal web depth. An array of six holes was also machined using a 5 mm diameter diamond-coated drill in both the tensile and compressive flanges. The holes were situated between the central loading pads, where the bending strains are maximum and constant, with three being on either half of the flange. The hole size was chosen so that the ratio of hole diameter to flange half-width, i.e. distance from flange edge to fillet radius of web, did not exceed 1:6 as recommended by the CRAG specifications[26] for avoiding the influence of free edges. The 12 holes were closed using plain shank bolts which were tightened to a torque of 5·4 Nm. This is representative of the manner in which a surface skin might be affixed to an array of such I-beams, or how a stiffener might be fixed to a large panel.

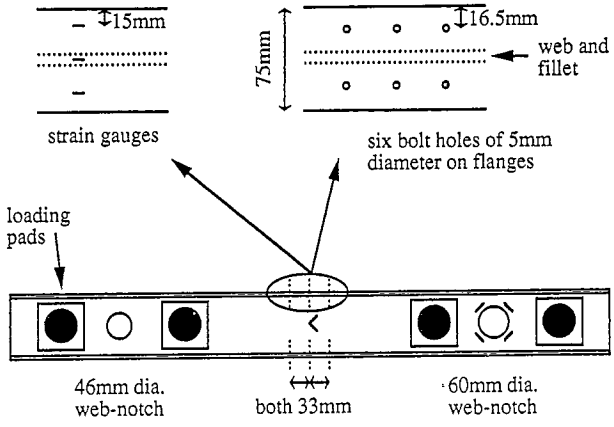

Fig. 3. Location of six closed bolt holes on the tensile and compressive flanges and two web cutouts on notched I-beams. The strain gauge positions are identified.

3 BEHAVIOUR OF I-BEAMS UNDER STATIC MECHANICAL LOADS

3.1 Introduction

All beams were loaded statically to failure under a displacement mode of control. As the applied load was increased from zero the beam response was initially linear elastic. Load, displacement and strain values were collated at increments of actuator load. Failure of the unnotched carbon/epoxy and glass/epoxy I-beams was concentrated around the compressive flange and initiated from regions of buckling. Failure of the notched carbon/epoxy and glass/epoxy I-beams initiated from the large web cutouts (i.e. from the 60 mm diameter hole).

At particular load levels the compressive flange region between the two pairs of central loading pads, where compressive flange strains were maximum, was

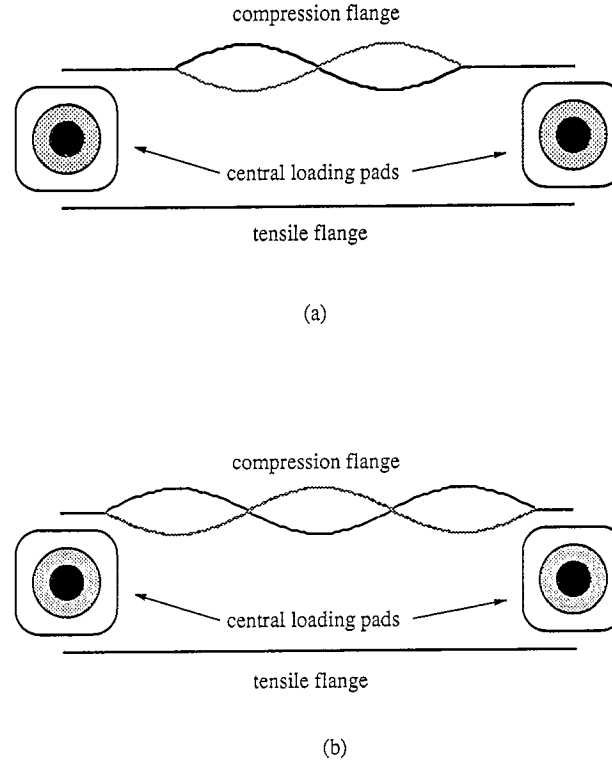

Fig. 4. Schematic diagram of the compression flange buckle for (a) the plain and notched carbon/epoxy beams and the plain glass/epoxy beam and (b) the notched glass/epoxy beam. Note that the free flange length between the central loading pads is 383 mm. The approximate amplitude and wavelength of each buckle is given in Table 3 (see also Fig. 5).

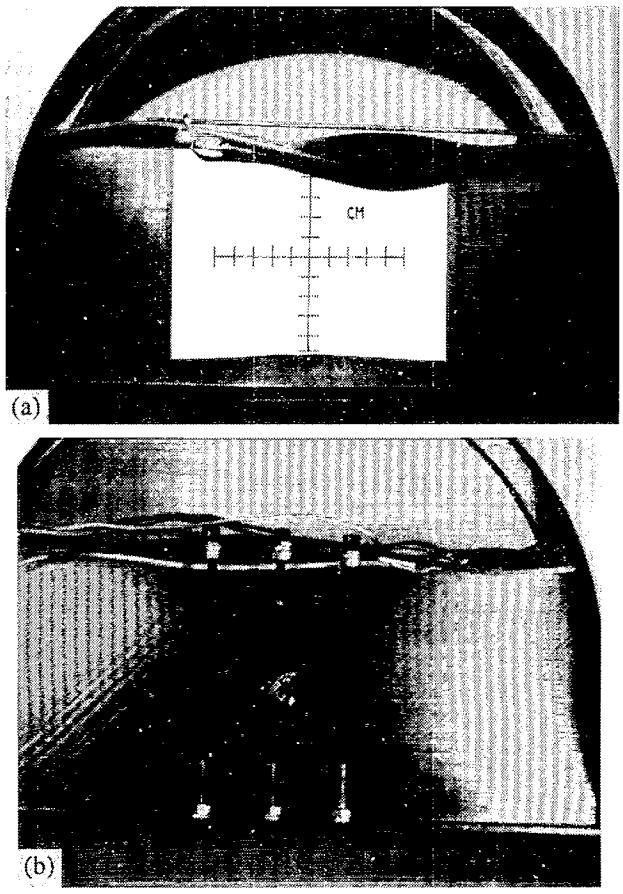

Fig. 5. Compression flange buckle for (a) the plain glass/epoxy I-beam and (b) the notched glass/epoxy beam. The buckling mode of the plain and notched carbon/epoxy beams are the same as that of the plain glass/epoxy beam given in (a) although the amplitudes and wavelengths are different. Note that the free flange length between the central loading pads is 383 mm. The bar markings in (a) are in cm. The bolts in (b) identify the positions of the filled flange holes. The approximate amplitude and wavelength of each buckle is given in Table 3 (see also Fig. 4).

observed to buckle in a mode that was antisymmetric across the flange width. This occurred on all I-beams, shown in Fig. 4 (schematically) and Fig. 5. The amplitude of the buckle increased to a maximum until failure. No other region of the beam was seen visually to buckle. The buckling and failure loads of each beam, together with the site from where failure initiated, are given in Table 2.

Table 2. Buckling and failure loads and regions of failure initiation of the I-beams

Beam	Buckling load (kN)	Failure load (kN)	Failure site
Unnotched carbon	55	96·0	Flange buckle
Notched carbon	55	74·0	Web cutout
Unnotched glass	35	74·8	Flange buckle
Notched glass	35	57·0	Web cutout

3.2 Buckling behaviour

When the buckle was first observed during the static test on the unnotched carbon/epoxy I-beam, i.e. at 55 kN, the node of the buckle was halfway along the length of the compressive flange (see Figs 4 and 5). The trough and crest of the buckle had maximum amplitude at the edges of the flange with zero amplitude at the intersection between the flange and web regions. Examination of the buckle across the flange width indicated that, for a crest which was situated at one edge of the flange, a trough was present at the directly opposite edge. As the actuator displacements increased the magnitude of the buckle increased visibly, until immediately preceding failure the amplitude of the buckle was almost 20 mm from crest to trough and the wavelength was some 280 mm. These compare with the free flange length of 383 mm between the central loading pads. It is difficult to say precisely where along the compression flange that the buckle failure initiated but from an examination of photographs taken during the test the damage appears to have initiated at or close to a crest, and corresponding trough, at the free edges of the flange. This is supported by fractographic observations[24] which indicate a peel site (i.e. mode I fracture) at the edge of the compression flange broadly corresponding to a crest/trough. This edge delamination subsequently propagated through to the web/flange junction between the central loading pads, across the web and towards the tensile flange. Failure could have initiated at this region due to local bending stresses in the compression flange arising from the buckling.

Figure 4 presents a schematic representation of the compressive flange buckle associated with the various I-beams immediately preceding failure whilst the approximate amplitude and wavelength of the buckles are given in Table 3. This information was not determined during testing but rather was obtained from photographs (such as Fig. 5) which had been taken during testing, and consequently is only approximate.

The carbon/epoxy beams and the unnotched E-glass/epoxy beams all buckled in a similar manner, as described above. However, the notched glass beam

Table 3. Approximate amplitude and wavelength of buckle on compressive flanges prior to failure; note that the free flange length between the central loading pads is 383 mm

Beam	Amplitude (mm)	Wavelength (mm)
Unnotched carbon	20	280
Notched carbon	12	256
Unnotched glass	18	264
Notched glass	13	250

buckled in a somewhat different manner. For this I-beam it was observed that there were three half-wavelengths to the buckle (as opposed to only two for the other beams) and that the midlength of the I-beam coincided with a crest/trough as opposed to a nodal position. However, in all cases, the buckles were antisymmetric across the width of the compression flange. The reason for this is not fully understood although theoretical modelling of the buckle[28] has predicted that the first and second eigenvalues are quite close together and, consequently, these two modes of buckling can occur for very similar values of applied actuator load. Moreover, the load distribution throughout the notched glass beam is not perfectly symmetric because of the different sizes of the two web cutouts and the layup that is antisymmetric about the midplane of the beam.

3.3 Damage in beams

Visual examination of the broken unnotched carbon/epoxy beam, after removal from the loading machine, showed the compressive flange and the web, but not the tensile flange, to be extensively damaged, with a predominance of delamination throughout the beam. Figures 6–8 indicate the visible extent of the damage in the compressive flange, the two faces of the web and the tensile flange. These photographs are of the central section of the beam. The various regions of the beam were subsequently C-scanned using ultrasonics to establish the extent of delamination: these findings have been marked on the beam and can be seen in the photographs. Whilst multiple delaminations were present, the most significant delaminations were between the backs of the C-sections and the Cs and flange caps, i.e. between the various manufacturing subcomponents. The fillet regions of the beam, i.e. the web/flange joint, were severely damaged with delaminations and matrix cracks present, as shown in Fig. 9.

Failure of the notched I-beams was localised around the large web holes and the damage associated with the notched carbon/epoxy and glass/epoxy I-beam cutouts is shown in Fig. 10. The directions of shear stress are identified in this figure so that the different damage mechanisms can be related to the components of local tensile and compressive stress. Within the carbon/epoxy beam (Fig. 10(a)) damage is seen to emanate along two diagonals from the cutout: one due to tensile stress and the other to compressive stress. The tensile fracture, from the cutout towards the tensile flange, has a clean straight appearance unlike the compressive fracture, from the cutout towards the compressive flange, which is more extensive and irregular. Extensive delamination, identified using ultrasonics, and fibre bridging are also associated with the compressive fracture. Damage within the E-glass/epoxy beam (Fig. 10(b)) shows some similarities with the carbon/epoxy beam although is actually quite different. Tensile and compressive damage are present in both material systems and these emanate outwards from the cutout. However, both the tensile and compressive damage are more extensive in the glass beam and all four quadrants are damaged (as opposed to only two for the carbon beam). The tensile fractures in the glass beam are cleaner than the compressive fractures although not as regular as in the carbon beam. Delamination and fibre bridging are also associated with the compressive fractures in the glass beam. Further fractographic details of these failures are to be given in future work.[24]

3.4 Measured loads and displacements

The measured actuator loads and displacements are presented in Fig. 11 as a standard P/δ plot for the four I-beams. The bending stiffness of the, nominally identical, carbon/epoxy beams was $9{\cdot}9 \pm 0{\cdot}5$ kN/mm whilst that of the E-glass/epoxy I-beams was $5{\cdot}9 \pm 0{\cdot}3$ kN/mm. Stiffness has been measured at the yoke/actuator positions and not at the position of maximum deflections, i.e. at the midspan of the beams. The load/deflection relationship for the unnotched carbon/epoxy I-beam is essentially linear until approximately 55 kN after which the beam exhibits increased compliance. The deviation from linearity in the load/deflection relationship was due to the onset of local buckling of the compressive flange,

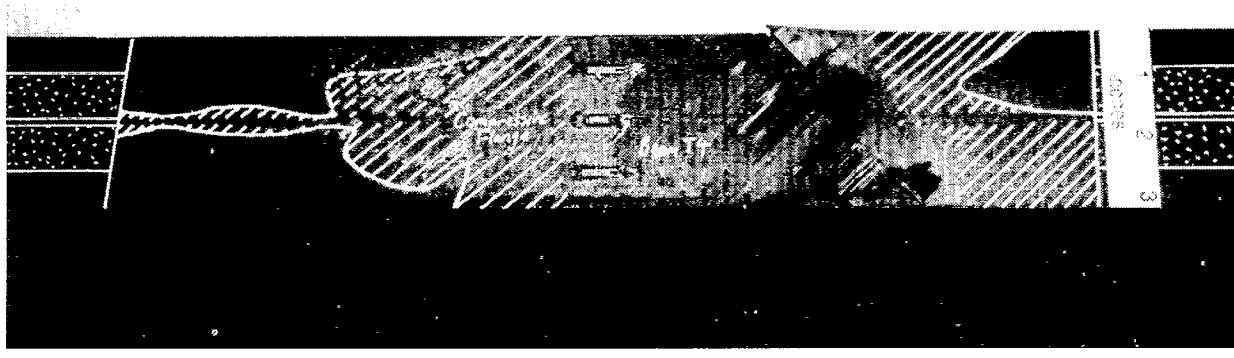

Fig. 6. Compressive flange damage of plain carbon/epoxy I-beam after failure. The shaded region identifies the extent of delamination between the central pairs of loading pads that was detected using ultrasonics.

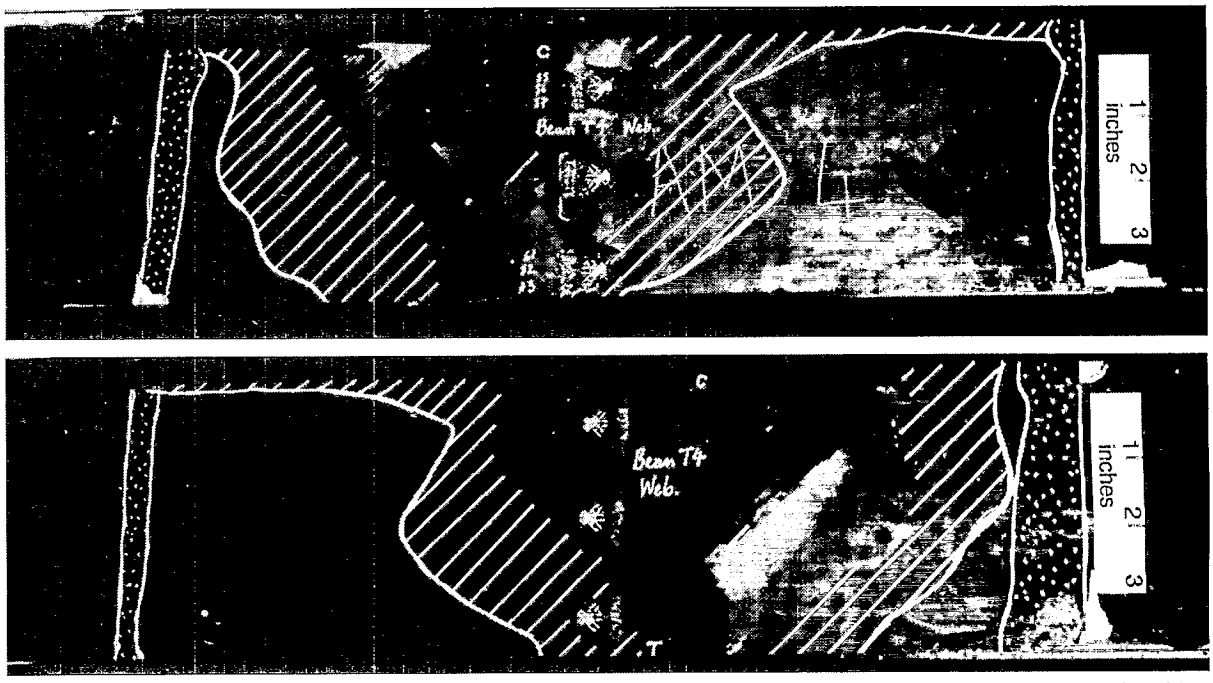

Fig. 7. Shear web damage of plain carbon/epoxy I-beam after failure. The two photographs identify the opposite sides of the beam. The shaded region identifies the extent of delamination between the central pairs of loading pads that was detected using ultrasonic A- and C-scanning. The compression and tension flanges are towards the top and bottom, respectively, in each photograph.

which increased directly with load up to failure, i.e. 96·2 kN. Further increases in the compliance of the various I-beams are due to increased buckling and the initiation and development of damage such as matrix cracking, delamination and fibre fracture.

3.5 Measured strains

Surface strains, which were measured in the web, tensile and compressive flange regions of the beam are given in Figs 12, 13 and 14, respectively. The position of the various strain gauges and shear rosettes are identified in Fig. 3. All rosettes have been sited along the neutral axis of the I-beams to measure shear strains. These have been placed between the central pairs of loading pads as well as between the outer pairs of loading pads and correspond to where shear strains are zero and constant, respectively. In some instances, rosettes were placed on opposite faces of the webs. Strain gauges have also been placed around the large web cutouts (i.e. 60 mm diameter) but not the small web holes (i.e. 45 mm diameter) in order to monitor the tensile and compressive strains up to fracture. These strain gauges, shown in Figs 3 and 12(c), are tangential to the edge of the cutout and are nominally 2–3 mm from the edge of the hole at angles of ±45° and ±135° orientation to the beam major axis. In some cases, gauges were placed on opposite faces of the web cutout and in others they were only situated so as to identify a single value of the tensile and compressive strains. Strain gauges were also used on the tensile and compressive flanges of the I-beams. These were only situated between the two pairs of central loading pads, as shown in Fig. 3, where the flange strains are maximum and constant. Only one gauge was used on the tensile flange and this was situated equidistant from the ends and edges of the flange. With regard to the compressive flange, up to five strain gauges were positioned equidistant from the ends of the flange: three on the top face of the flange and two on the underside of the flange. On the top face of the compressive flange, one of the three gauges was at the midpoint across the width whilst the other

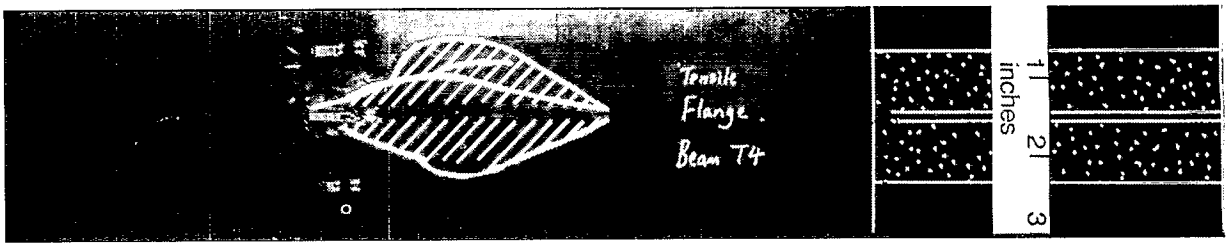

Fig. 8. Tensile flange damage of plain carbon/epoxy I-beam after failure. The shaded region identifies the extent of delamination between the central pairs of loading pads that was detected using ultrasonics.

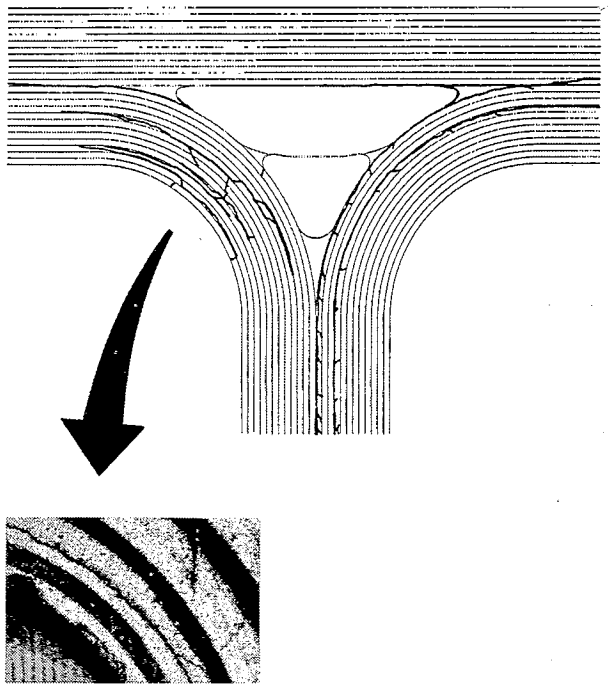

Fig. 9. Damage in the fillet region, i.e. the web/tensile flange region, of plain carbon/epoxy I-beam failure. (Darker lines indicate regions of delamination and matrix cracking.)

two were nominally 15 mm from the two edges of the flange. The two gauges on the undersides of the flange were directly opposite the two gauges that were 15 mm from the edges of the flange. Differences in the recorded strain levels of these five gauges identify different degrees of flange buckling, as discussed below.

The shear strains detailed in Fig. 12 are from three distinct regions of the web, i.e. the two areas between the outer loading pads at both ends of the beam and the single region between the two central pairs of loading pads. Under four-point bending, the shear between the central region is zero whilst it is equal and opposite within the two outer regions. What is interesting to observe is that when flange buckling occurs, the beam cross-section is, effectively, no longer symmetric and this is detected by the shear rosettes within the central web region when a non-zero shear strain is recorded, as shown in Fig. 12(b). Furthermore, the shear strains between the outer loading pads continue to increase in an essentially linear manner at load levels which exceed the buckling load, right up to ultimate failure of the beam. Since the buckling was only noted between the central loading pads on the beam, i.e. the longest region of unreinforced compressive flange, and did not extend beyond this region, it is not surprising that the shear strains in the outer web regions of the beam continued to increase linearly at loads up to the failure load, as shown in Fig. 12(a). The strains around the large web cutouts, i.e. the notched carbon/epoxy and glass/epoxy I-beams, are given as tensile and compressive components in Fig. 12(c). Since failure of the notched I-beams occurs around the web cutouts, it is these strain gauges which record the greatest levels of strain. Maximum direct strains around the carbon cutout are 0·94 and −0·99% whilst the corresponding strains around the glass cutout are 1·40 and 1·38%, as detailed in Table 4. These levels of strain are greater than those recorded elsewhere in the notched beams because of the stress concentration effect of the cutout. It is worth considering the compressive strains around the web cutouts, shown in Fig. 12(c). There is some divergence in the direct strains recorded by gauges on opposite surfaces of the I-beam at 50 kN for the notched carbon/epoxy I-beam and at 40 kN for the notched glass/epoxy I-beam. The reason for this is not known although it could be associated either with slight misalignments of strain gauges or with web buckling. It is more probably due to buckling since the gradient of the change in strains with load deviates from linearity at these particular loads.

The strains which were recorded on the tensile and compressive flanges are detailed in Figs 13 and 14 whilst the positions of the corresponding strain gauges are given in Fig. 3 and have been detailed above. The tensile flange strains increase almost linearly with increasing load and, as with the shear strains in the outer web regions, this indicates the absence of any buckling in this area of the beam. Buckling of the compressive flange is, however, clearly recorded by the strain gauges which were sited on this flange, as can be seen in Fig. 14, where the strains bifurcate at the onset of buckling. Those gauges which were on the concave side of the buckle recorded higher levels of compressive strain whilst those on the convex face had some degree of tensile strain superimposed on a predominantly compressive strain and consequently recorded a lower level of compressive strain. Maximum strain levels of −0·84 and 1·27% were recorded in the compressive flange and the tensile flange of the unnotched carbon/epoxy and glass/epoxy I-beams, respectively. These strains are less than the carbon- and glass-fibre failure strains. However, since failure of the unnotched I-beams did not initiate from the location of the strain gauges, this is only to be expected. Furthermore, in the case of the unnotched glass/epoxy I-beam, the maximum strain of 1·27% was recorded in the tensile flange whilst failure initiated in the compressive flange. However, this must be viewed together with the fact that the strain gauges on the compressive flange were actually sited along the node of the buckle and therefore did not record the maximum levels of strain which existed within the compressive flange.

Table 4 identifies the maximum direct tensile and compressive strains which were measured during each test and may be compared against the failure strains of the carbon- and glass-fibres of 1·5[29] and 2·4%.[30]

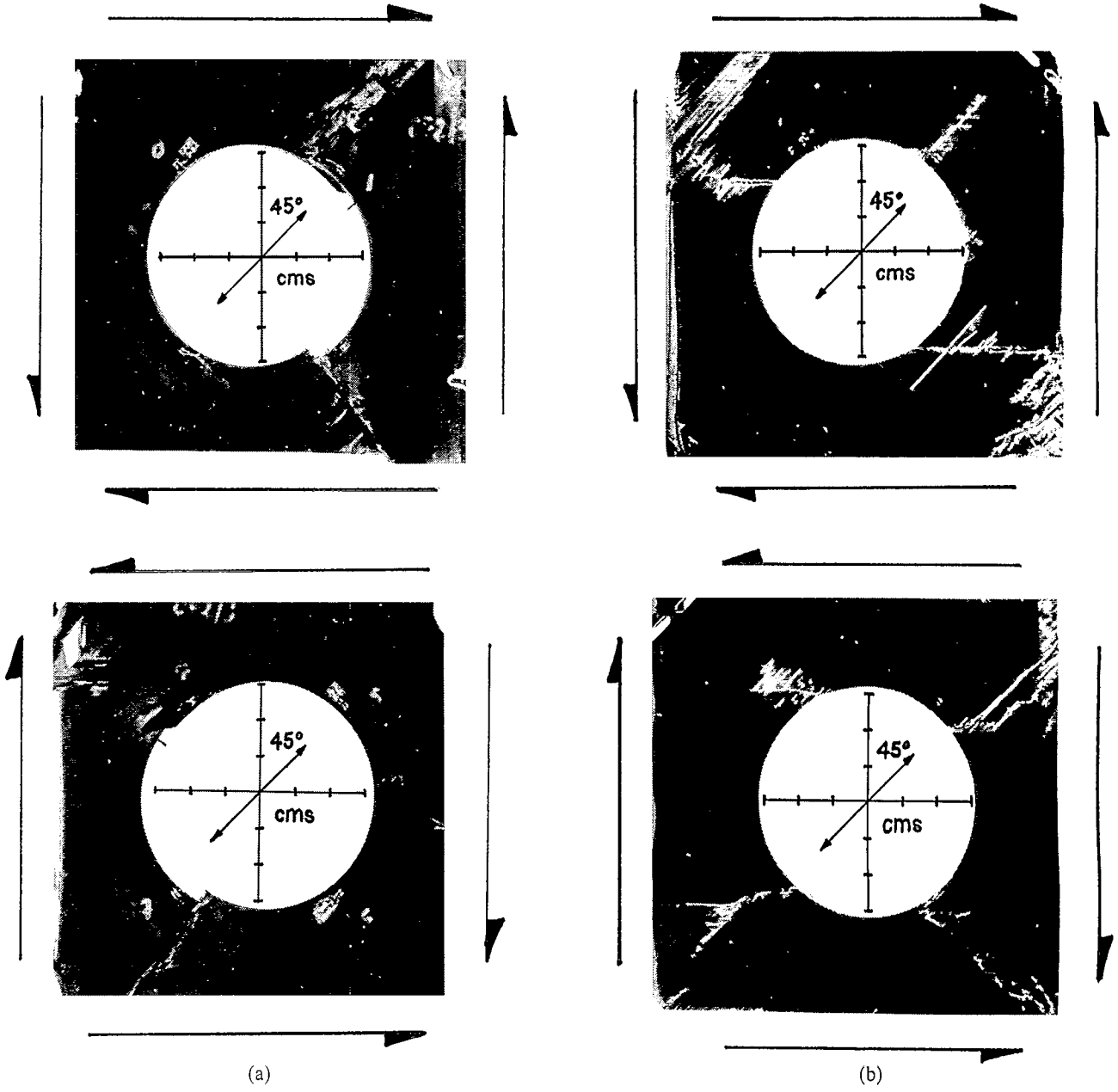

Fig. 10. Damage around large web cutout (i.e. 60 mm diameter) after failure of (a) the notched carbon/epoxy I-beam and (b) the glass/epoxy I-beam. Front and back faces are identified together with the directions of shear stress. The bar markings are in cm and the +45° direction identifies the orientation of the top surface ply.

4 PREDICTIONS OF I-SECTION BEHAVIOUR

Using simple bending theory the overall behaviour of the beam was calculated. For example, the deflection at the quarter positions of the carbon/epoxy beam, i.e. yoke deflection, at the onset of buckling was predicted to be 5·00 mm:

$$\delta_{\text{yoke}} = \frac{Pa^2}{2EI}\left(\frac{a}{3}+\frac{L}{2}\right) \tag{1}$$

where $a = 0{\cdot}25$ m, $L = 0{\cdot}5$ m, $P = 55$ kN, $E = 54{\cdot}75$ GPa and $I = 2{\cdot}0961 \times 10^6$ mm^4. This may be compared to the experimentally measured yoke displacement of 5·8 mm, shown in Fig. 11, which includes link extension and bearing deflection and is consequently greater than that predicted from beam theory. This predicted deflection of 5·0 mm has been calculated solely by considering the flexure of the beam. However, it is possible to obtain an approximate estimate of the deflection due to shear stress,[31] δ_{shear}, and consequently a more realistic estimate of the total yoke deflection:

$$\delta_{\text{sheer}} = \frac{6}{5}\frac{(P/2)a}{AG} \tag{2}$$

where, at the onset of buckling in the unnotched carbon/epoxy I-beam, $P = 55$ kN, $a = 0{\cdot}25$ m, $A \approx 125 \times 3$ mm^2 and $G \approx 24{\cdot}8$ GPa (as calculated using LAP[25]). Consequently, $\delta_{\text{shear}} = 0{\cdot}89$ mm. This would predict a more accurate estimate of the yoke deflection as being some 5·89 mm, i.e. the sum of the

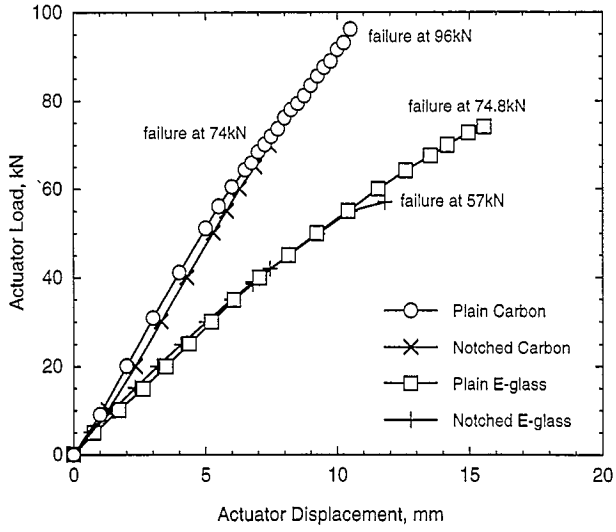

Fig. 11. Load/displacement (P/δ) plots for plain and notched carbon/epoxy and E-glass/epoxy I-beams.

contributions due to flexure and shear. This is quite an acceptable agreement with the experimentally measured yoke displacement of 5·8 mm. The theoretical value of the maximum, midlength deflection of the

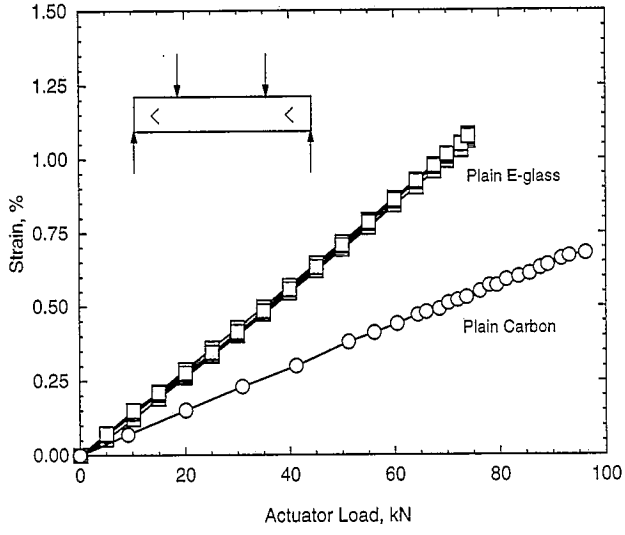

(a)

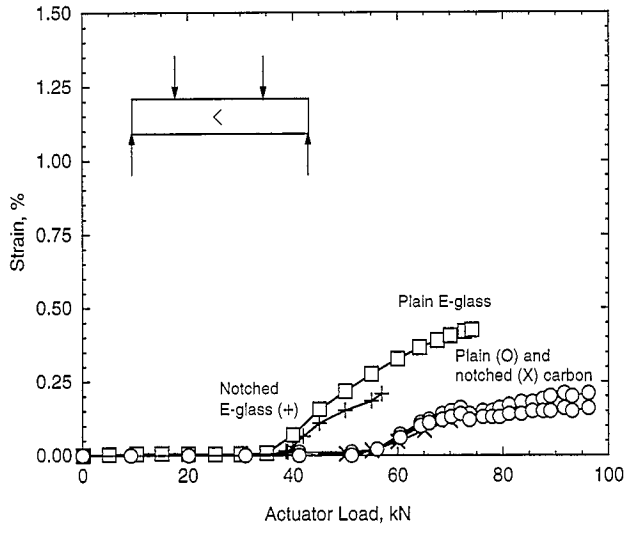

(b)

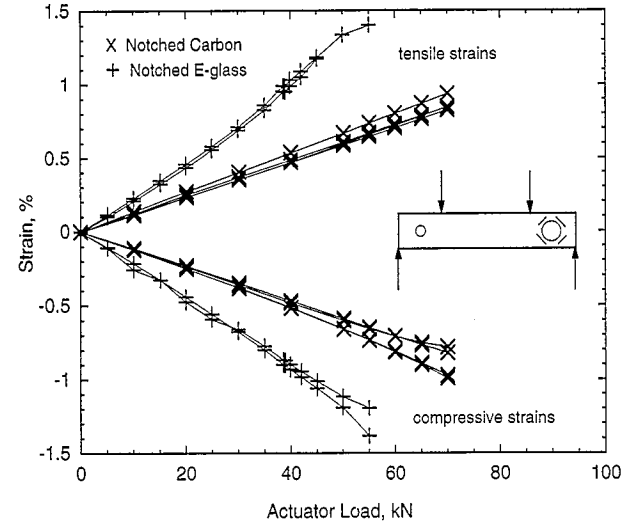

(c)

Fig. 12. (a) Web strains of plain carbon/epoxy and E-glass/epoxy I-beams. The strain gauges are positioned along the neutral axis and are centrally located between the two pairs of outer loading pads. The strains increase linearly from zero with increasing applied actuator load. (b) Web strains of plain and notched carbon/epoxy and E-glass/epoxy I-beams. The strain gauges are positioned along the neutral axis and are centrally located between the two pairs of middle loading pads. The non-zero strains identify the loads at which beam buckling occurs (35 and 55 kN for the E-glass/epoxy and carbon/epoxy I-beams, respectively). (c) Web strains of notched carbon/epoxy and E-glass/epoxy I-beams around large web cutout. Tensile and compressive strains are measured some 2–3 mm from the edge of the cutout along the ±45° lines from the centre of the cutout.

Fig. 12. (*Continued.*)

carbon/epoxy beam is consequently predicted by classical beam theory as being $\delta_{max} = (11/8)\delta_{yoke} + 0{\cdot}89$ (the shear deflection) = 7·77 mm.

Similar calculations for the unnotched E-glass/epoxy I-beam predicts the yoke deflection as being 8·84 mm. This is based on both the flexure and shear contributions which have been calculated as being 6·52 and 2·32 mm, respectively. This total yoke deflection of 8·84 mm is an overprediction by some 45% of the 6·07 mm that was measured experimentally as has already been identified in Fig. 11.

The compressive flange strain between the inner loading pads at which local buckling occurs was calculated using

$$\epsilon_b = \frac{K}{1-\nu^2}\left(\frac{t}{b}\right)^2 \tag{3}$$

derived for isotropic materials.[32] For the present

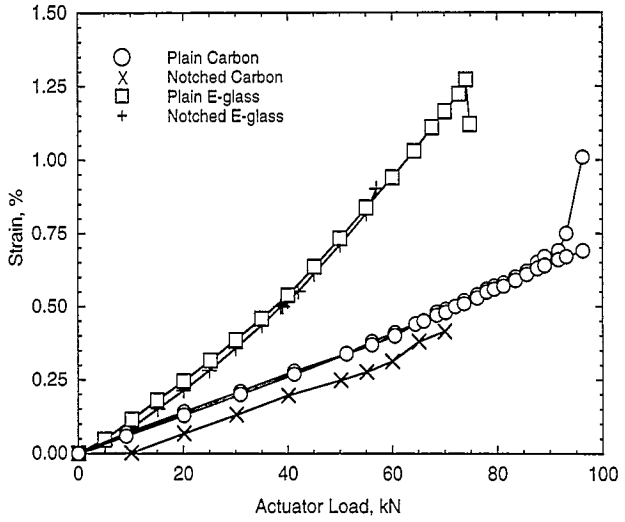

Fig. 13. Tensile flange strains of plain and notched carbon/epoxy and E-glass/epoxy I-beams. The strain gauges were sited between the central pairs of loading pads.

beams ($b = 36$ mm, $t = 3$ mm, $\nu = \nu_{12}$ for unidirectional layup) this gives strains of 0·32% for both carbon/epoxy and glass/epoxy when $K = 0{\cdot}416$[32] and 0·44% when $K = 0{\cdot}58$.[33] K has been chosen for the case of a panel with three edges simply supported and one edge free. Experimental buckling strains were 0·4% for both materials (see Fig. 14(a) and (c)). The predicted buckling strains, ϵ, can be related to P since the stress within the flange is given by:

$$\sigma = E_{11}\epsilon = \frac{[(P/2)a]y}{I} \tag{4}$$

For the carbon/epoxy beam these strains correspond to predicted loads at buckling of 48·2 and 66·2 kN respectively, which compare with the 55 kN found experimentally. For the glass/epoxy beam the corresponding loads are 23·5 and 32·3 kN, compared to an experimental value of 35 kN. There is clearly better agreement for the predicted buckling loads of the carbon/epoxy beam than for the glass/epoxy component, although the error in the predicted buckling load is less than 10%.

Although these predicted and measured loads are in reasonable agreement, it was observed that final fracture did not occur in a simple fashion, i.e. it was either by local flexure of a buckled flange, or from the edge of a cutout. Therefore, it was decided that it would be inappropriate to use laminate analysis together with a stress-based failure criterion. Issues relating to this topic are addressed in the second paper of this series.[28]

5 DISCUSSION

Buckling of the unnotched and notched I-beam occurred at the same levels of actuator load. For the carbon/epoxy and E-glass/epoxy beams, these are identified in Table 2 as 55 and 35 kN, respectively. However, it should be emphasised that these experimental loads are probably only accurate to within ±2 kN, since the load was increased during the displacement controlled tests in increments of 5 kN. The onset of buckling was deduced by observing the beam flanges during testing and by identifying the deviation of the strains from linearity, as shown in Figs 12(b) and 14.

The failure loads, as distinct from the buckling loads, were far more easily identified by the catastrophic fracture of an I-beam. Since the static tests were performed under displacement control, the I-beams did not completely disintegrate: fracture was contained around the web cutout for the notched beams, for example, and the beams were still able to sustain some small load (a non-zero load that was less than the load at which fracture had occurred). However, such events were deemed to define failure since no extra increased loading above this fracture load could be sustained by a beam. It is worth noting that there was almost no acoustic evidence of damage prior to failure of the E-glass/epoxy beams whilst failure of the carbon/epoxy beams was preceded by increasing amounts of audible cracking.

The direct tensile and compressive strains given in Figs 12–14 correspond to values recorded at the strain gauge positions identified in Fig. 3. Unless failure occurs at the precise location of a particular strain gauge, the measured direct strain will be less than the fibre failure strain, which is 1·5 and 2·4% for the carbon and E-glass fibres, respectively. In every case, it is seen that the recorded strain levels are less than the fibre failure strains. For instance, failure of the unnotched carbon/epoxy I-beam occurs on the compressive flange where the maximum strain recorded was −0·84% (channel 2 of Fig. 14(a)). This particular strain gauge was actually situated on the middle of the top face of the flange. Failure actually initiated from the flange edge and, moreover, the position of this particular strain gauge did not coincide with the crest/trough of the buckle on the flange: rather, it coincided with a nodal position on the buckle. From an approximate measure of the curvature of the buckle prior to failure, the buckling strain on the compression flange of the unnotched carbon/epoxy I-beam was calculated as being $-0{\cdot}75 \pm 0{\cdot}10\%$:

$$\epsilon_b = \frac{t/2}{R} = -0{\cdot}75\% \tag{5}$$

The average strain within the compression flange prior to failure, i.e. excluding the influence of the buckle, along the midplane of the compression flange, was −0·57% (channels 3 and 5 record direct strains of −0·78 and −0·36% prior to failure as shown in Fig. 14(a)). Consequently, the maximum strain on the

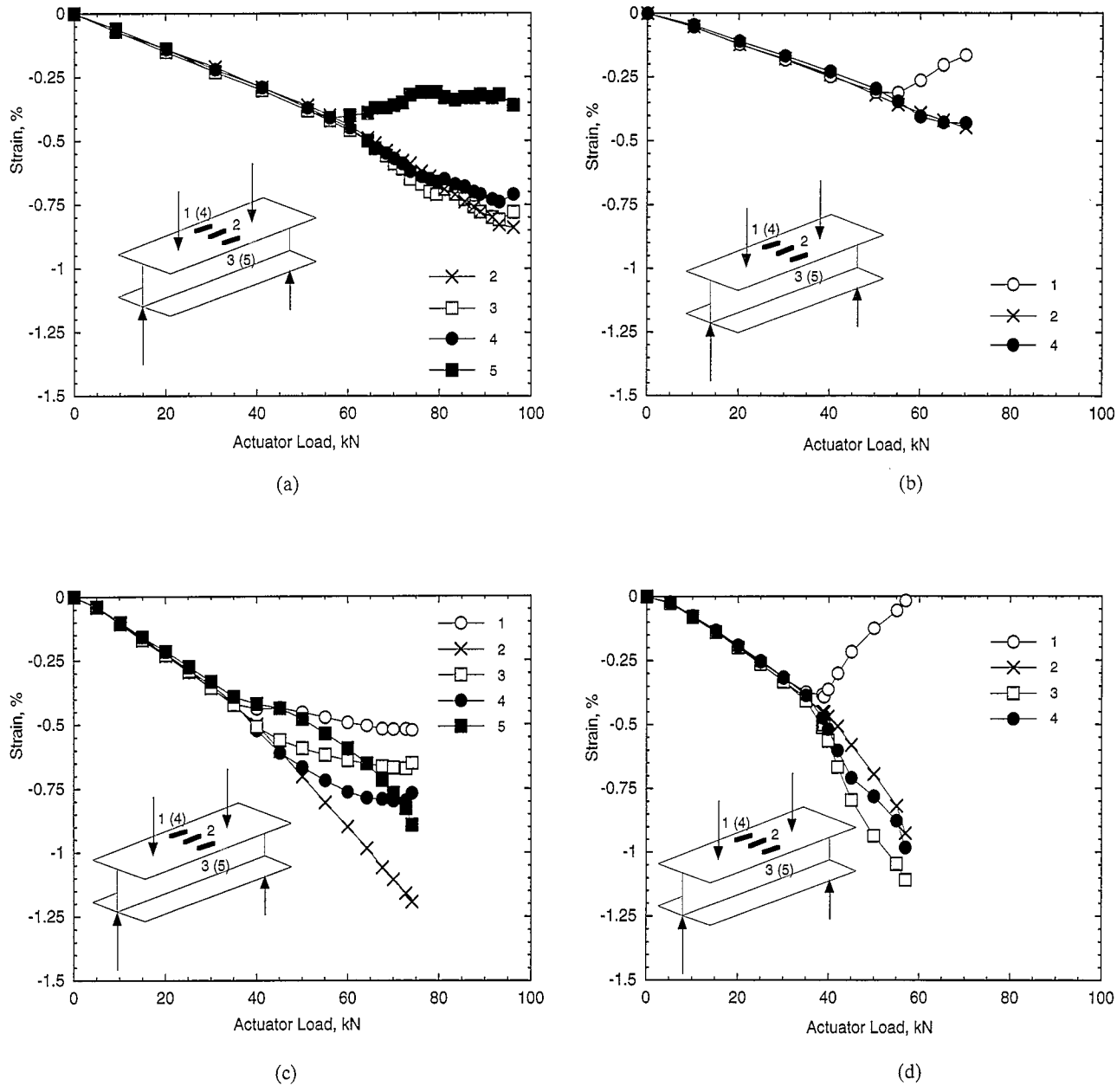

Fig. 14. (a) Compressive flange strains of plain carbon/epoxy I-beam. Five strain gauges were sited halfway along the length of the beam on the top (channels 1, 2 and 3) and bottom (channels 4 and 5) faces of the compressive flange. The strain gauges corresponding to channels 4 and 5 are opposite those corresponding to channels 1 and 3, respectively. One gauge was in the middle of the flange (channel 2) whilst the other four were nominally 15 mm from the edge of the flange as shown in Fig. 3. Channel 1 failed during testing and consequently no results for this gauge are presented. (b) Compressive flange strains of notched carbon/epoxy I-beam. Five strain gauges were sited halfway along the length of the beam on the top (channels 1, 2 and 3) and bottom (channels 4 and 5) faces of the compressive flange. The strain gauges corresponding to channels 4 and 5 are opposite those corresponding to channels 1 and 3, respectively. One gauge was in the middle of the flange (channel 2) whilst the other four were nominally 15 mm from the edge of the flange as shown in Fig. 3. Channels 3 and 5 failed during testing and consequently no results for these gauges are presented. (c) Compressive flange strains of plain E-glass/epoxy I-beam. Five strain gauges were sited halfway along the length of the beam on the top (channels 1, 2 and 3) and bottom (channels 4 and 5) faces of the compressive flange. The strain gauges corresponding to channels 4 and 5 are opposite those corresponding to channels 1 and 3, respectively. One gauge was in the middle of the flange (channel 2) whilst the other four were nominally 15 mm from the edge of the flange as shown in Fig. 3. (d) Compressive flange strains of notched E-glass/epoxy I-beam. Five strain gauges were sited halfway along the length of the beam on the top (channels 1, 2 and 3) and bottom (channels 4 and 5) faces of the compressive flange. The strain gauges corresponding to channels 4 and 5 are opposite those corresponding to channels 1 and 3, respectively. One gauge was in the middle of the flange (channel 2) whilst the other four were nominally 15 mm from the edge of the flange as shown in Fig. 3. Channel 5 failed during testing and consequently no results for this gauge are presented. The deviation in strain values at approximately 55 kN (a,b) or 35 kN (c,d) identifies the onset of flange buckling.

Table 4. Magnitude and location of maximum direct strains during static tests

Beam	Max. tensile strain (%)	Max. compressive strain (%)
Unnotched carbon	0·75 (tensile flange)	−0·84 (comp. flange)
Notched carbon	0·94 (web cutout)	−0·99 (web cutout)
Unnotched glass	1·27 (tensile flange)	−1·19 (comp. flange)
Notched glass	1·40 (web cutout)	−1·38 (web cutout)

compression flange is the sum of the buckling strain, ϵ_b, and the average strain, ϵ_{avg}:

$$\hat{\epsilon} = \epsilon_b + \epsilon_{avg} = -1{\cdot}32 \pm 0{\cdot}10\% \quad (6)$$

This agrees reasonably well with the 1·5% failure strain for the carbon/fibre. A similar analysis for the E-glass/epoxy I-beam prior to failure reveals that the average strain was between −0·65% (average of channels 1 and 4) and −0·77% (average of channels 3 and 5) whilst the buckling strain was approximately −1·25%. Consequently, the maximum strain on the compressive flange of the unnotched E-glass/epoxy I-beam prior to buckling was approximately $-2{\cdot}0 \pm 0{\cdot}1\%$. This compares reasonably well with the fracture strain of the E-glass fibres of 2·4%. These estimates of strain prior to fracture of the carbon/epoxy and glass/epoxy I-beams are based upon the buckle curvature as measured from photographs and strain gauge readings, both of which were recorded prior to fracture, rather than at the precise instant of fracture. Consequently, these estimates are somewhat below the actual fibre fracture strain levels that have been provided by materials manufacturers.[29,30]

The notched I-beams failed along the tensile and compressive diagonals of the large web cutouts, as shown in Fig. 10. Failure initiated from the edge of the large cutout due to local tensile stresses. Within the glass/epoxy beam, the maximum direct tensile and compressive strains closest to these positions were 1·40 and −1·38%, compared to the E-glass-fibre failure strain of 2·4%. The reason for this difference is due to the fact that the strain gauges were not positioned directly at the site of failure initiation, i.e. at the boundary of the cutout. The strain gauge readings were averaged over the area of the actual gauges, which had been positioned some 2–3 mm from the edge of the cutout, whereas fracture initiated from the edge of the cutout. Whilst the stress field in the vicinity of the cutout is complicated, it is possible to establish some order of magnitude for the stresses and strains that exist at the edge of the cutout from the known levels of strain some 2–3 mm ahead of the cutout.[30] The strains at the edge of the cutout are calculated to be approximately $1{\cdot}9 \pm 0{\cdot}1\%$ for the E-glass/epoxy beam and $1{\cdot}5 \pm 0{\cdot}1\%$ for the carbon/epoxy beam and compare reasonably well with the fibre fracture strains of 2·4 and 1·5%, respectively. Details of these calculations are given in the Appendix.

The calculations for buckling loads and displacements using simple bending theory agree well with experimental results when the calculated displacements include shear effects. The results for flange buckling are less satisfactory. Partly this is because of the lack of agreement in the literature for isotropic materials. Also, of course, the layup used in the beams is not even quasi-isotropic, so appropriate allowance should be made in the theory when calculating the buckling coefficient, K. A further, related, issue is the degree of constraint afforded at the web/flange junction to flange deformation; this issue will be addressed in a later paper.[28]

6 CONCLUSIONS

The mechanical behaviour of both unnotched and web- and flange-notched continuously reinforced carbon/epoxy and glass/epoxy I-beams has been investigated. The global static response and ultimate failure due to static mechanical loads under four-point flexure has been described in terms of strains, compliance, buckling and final fracture.

A mode of buckling that was antisymmetric across the width of the compressive flange was observed prior to failure in all cases. Two different mode shapes were observed: the lower eigenvalue defined a mode that was antisymmetric along the beam length and had two half-wavelengths whilst the second mode was symmetric along the beam length and had three half-wavelengths between the pairs of inner loading pads. Buckling and failure of the unnotched and notched glass/epoxy beams occurred at loads that were approximately 75% of the corresponding loads in the carbon/epoxy beams whilst buckling of both the unnotched carbon/epoxy and glass/epoxy beams occurred at loads that were approximately 50% of the failure loads of the unnotched beams.

Failure of the unnotched I-beams was concentrated around the compressive flange buckle and initiated, due to local tensile, Mode I stresses, at the flange edge close to a crest/trough on the buckle. Fracture subsequently propagated from this initiation site throughout the compressive flange and web regions. Failure of the notched I-beams, on the other hand, initiated from a shear loaded cutout within the web at loads that were approximately 75% of the unnotched beam failure loads. Tensile and compressive damage, in the form of matrix cracking, fibre fracture and delamination occurred due to the local tensile and compressive stresses within the web region.

Direct strains were recorded throughout the I-beams up to failure. For both compressive and tensile fracture, these direct recorded strains were

found to correlate reasonably well with the failure strains of both the carbon and glass fibres. For example, a maximum direct compressive strain level of −0·84% was measured prior to failure on the compressive flange of the unnotched carbon beam. This strain reading was associated with a strain gauge that corresponded to a position that was close to a node on the flange buckle and a more accurate estimate of the maximum strain at the failure site of this beam (crest/trough of buckle on the edge of the compression flange) was provided by the sum of the strain associated with the curvature of the buckle, $\epsilon_b = -0{\cdot}75\%$, and the average strain through the thickness of the compression flange, $\epsilon_{avg} = -0{\cdot}57\%$. In other words, the maximum strain at the site of failure initiation $\hat{\epsilon} = \epsilon_b + \epsilon_{avg} = -1{\cdot}32 \pm 0{\cdot}10\%$. This compares acceptably well with the failure strain of the carbon fibres of 1·5%. For the unnotched E-glass/epoxy beam, the corresponding maximum compressive flange strain at the site of failure initiation was measured as being $-2{\cdot}0 \pm 0{\cdot}1\%$ compared with a failure strain of the E-glass fibres of 2·4%.

Similarly, a maximum direct tensile strain level of 1·40% was measured some 2–3 mm ahead of the web cutout in the notched glass beam. Fracture in this component initiated from the boundary of the cutout due to local tensile stresses. A simple closed form relationship between the distance from a cutout and the strain at that particular point was used to provide some estimate of the order of magnitude for the strain that would exist at the edge of the cutout from the known level of strain, 1·4%, some 2–3 mm ahead of the cutout. The strains at the edge of the cutout in the glass/epoxy beam were predicted to be approximately $1{\cdot}9 \pm 0{\cdot}1\%$; this is approximately 20% less than the glass-fibre fracture strains of 2·4%. The strain at the edge of the web cutout in the carbon/epoxy beam was similarly predicted as being $1{\cdot}5 \pm 0{\cdot}1\%$ compared with the fibre failure strain level of 1·5%.

Shear strains within the unnotched beams were also monitored during testing. Between the central loading pads, the strains along the beam neutral axis were correctly measured as zero until buckling occurred, after which non-zero strains were recorded. Between the outer pairs of loading pads, on the other hand, the shear strains increased linearly with increasing applied actuator load until failure of the beams occurred.

Isotropic beam theory was used to predict the deflections, strains and loads at which buckling occurred in the unnotched I-beams. Displacement at buckling was predicted to be 5·89 mm at the central loading points for the carbon/epoxy beams and this compared with 5·8 mm measured experimentally. This prediction included shear effects, although the greater amount of beam displacement was due to flexure rather than to shear. The predictions for buckling load and strain were in good agreement with the response of the carbon/epoxy I-beams but the buckling load for the E-glass/epoxy I-beam was underpredicted by almost 10%.

Future papers in this series will discuss the use of numerical modelling procedures to predict the I-beam behaviour and present the results of a fractographic analysis of the failure sequence and characteristics of the I-beams. The fatigue behaviour of the I-beams and a generic modelling strategy for predicting the behaviour of such structural components using fracture mechanics concepts and simple laboratory specimens will be considered.

ACKNOWLEDGEMENTS

The authors acknowledge the financial assistance of British Aerospace plc, the DTI (via the LINK 'Structural Composites' programme), EI Du Pont de Nemours & Co. Inc., Rolls Royce plc, SERC, Shell Research and Westland Helicopters Ltd, as well as the advice of Prof. P. Curtis of DRA. This work was performed when M.D.G. was at Imperial College. The assistance throughout this experimental programme of Mr E. W. Godwin and Mr H. J. MacGillivray of Imperial College is acknowledged.

REFERENCES

1. Chandra, R. & Chopra, I., Experimental and theoretical analysis of composite I-beams with elastic couplings. *AIAA J.*, **29** (1991) 2197–206.
2. Gamziukas, V., Skjuvprov med I-balkar av kolfiberarmerad plast med urtag i livet. FFA Report TN 1986-78, Aeronautical Research Institute of Sweden (FFA), 1986 (in Swedish).
3. Hollmann, K., Failure analysis of a shear loaded graphite/epoxy beam containing an irregular cutout. *Engng Fract. Mech.*, **39** (1991) 159–75.
4. Smith, S. J. & Bank, L. C., Modifications to beam theory for bending and twisting of open section composite beams—Experimental verification. *Comp. Struct.*, **22** (1992) 169–77.
5. Purslow, D., Composites fractography without an SEM—The failure analysis of a CFRP I-beam. *Composites*, **15** (1984) 43–8.
6. Kedward, K. T., Wilson, R. S. & McLean, S. K., Flexure of simply curved composite shapes. *Composites*, **20** (1989) 527–36.
7. Greenhalgh, E. S., Some fractographic investigations of carbon-fibre reinforced thermoplastic I-beams (unpublished results).
8. Greenhalgh, E. S., Mechanical evaluation of carbon-fibre reinforced thermoplastic I-beams. DRA TR 92071, Farnborough, UK, 1993.
9. Mandell, J. F. & Meier, U., Effects of stress ratio, frequency and loading time on the tensile fatigue of glass-reinforced epoxy. *Long-Term Behaviour of Composites*, ASTM STP 813, ed. T. K. O'Brien. American Society for Testing and Materials, Philadelphia, PA, 1983, pp. 55–77.
10. Meier, U., Mueller, R. & Puck, A., FRP-box beams under static and fatigue loading. *Proc. Int. Conf. on*

Testing, Evaluation and Quality Control of Composites, TEQC83, ed. T. Feest. Surrey University, Guildford, UK, 13–14 September 1983, pp. 324–36.
11. Gilchrist, M. D., Godwin, E. W., Kinloch, A. J., MacGillivray, H. J. & Matthews, F. L., Fatigue behaviour of composite structural members. *Proc. 2nd Int. Conf. on Deformation and Fracture of Composites*, UMIST, Manchester, UK, 29–31 March 1993.
12. Gilchrist, M. D., Kinloch, A. J., Matthews, F. L. & Osiyemi, S. O., Fatigue performance of composite structural I-beams. *Proc. ECCM-6,* Bordeaux, France, 20–24 September 1993.
13. Allen, H. G. & Bulson, P. S., *Background to Buckling*, McGraw-Hill, 1980.
14. Mottram, J. T., Structural properties of a pultruded E-glass-fibre-reinforced polymeric I-beam. *Proc. 6th Int. Conf. on Composite Structures*, ed. I. H. Marshall. Elsevier Applied Science, London, 1991, pp. 1–28.
15. Mottram, J. T., Evaluation of design analysis for pultruded fibre-reinforced polymeric box beams. *The Structural Engineer*, **69**(11) (1991) 211–20.
16. Mottram, J. T., Lateral–torsional buckling of a pultruded I-beam. *Composites*, **23** (1992) 81–92.
17. Mottram, J. T., Lateral–torsional buckling of thin-walled composite I-beams by the finite difference method. *Comp. Engng*, **2** (1992) 91–104.
18. Miller, A. G. & Wingert, A. L., Fracture surface characterization of commercial graphite/epoxy systems. *Nondestructive Evaluation and Flaw Criticality for Composite Materials,* ASTM STP 696, ed. R. B. Pipes. American Society for Testing and Materials, Philadelphia, PA, 1979, pp. 223–73.
19. Morris, G. E., Determining fracture directions and fracture origins on failed graphite/epoxy surfaces. *Nondestructive Evaluation and Flaw Criticality for Composite Materials,* ASTM STP 696, ed. R. B. Pipes. American Society for Testing and Materials, Philadelphia, PA, 1979, pp. 274–97.
20. Purslow, D., Some fundamental aspects of composites fractography. RAE TR 81127, October 1981.
21. Purslow, D., Matrix fractography of fibre-epoxy composites. RAE TR 86046, July 1986.
22. Zenkert, D., Effect of manufacture-induced flaws on the strength of foam core sandwich beams. *Damage Detection in Composite Materials,* ASTM STP 1128, ed. J. E. Masters. American Society for Testing and Materials, Philadelphia, PA, 1992, pp. 137–51.
23. Iyengar, N. G., *Structural Stability of Columns and Plates*, Ellis-Horwood, 1988.
24. Gilchrist, M. D., Kinloch, A. J. & Matthews, F. L., Static behaviour of carbon-fibre- and glass-fibre-reinforced epoxy I-beams: III. Fractographic failure observations (in prep.).
25. LAP: Laminate Analysis Program, Centre for Composite Materials, Imperial College, London, 1991.
26. Curtis, P. T. (ed.), CRAG test methods for the measurement of the engineering properties of fibre reinforced plastics. RAE TR 88012, 1988.
27. Ahlstrom, L. M. & Bäcklund, J., Shape optimization of openings in composite pressure vessels. *Comp. Struct.*, **20** (1992) 53–62.
28. Gilchrist, M. D., Kinloch, A. J., Matthews, F. L. & Wang, Y., Static behaviour of carbon-fibre- and glass-fibre-reinforced epoxy I-beams: II. Finite element predictions (in prep.).
29. Lovell, D. R., *Carbon and High Performance Fibres Directory*, 5th edn, Chapman & Hall, 1991.
30. Agarwal, B. D. & Broutman, L. J., *Analysis and Performance of Fibre Composites*, Wiley, 1990.
31. Benham, P. P. & Warnock, F. V., *Mechanics of Solids and Structures*, Pitman, London, 1973.
32. Roark, R. J., *Formulas for Stress and Strain*, McGraw-Hill, New York, 1954.
33. *Handbook of Aeronautics, No. 1: Structural Principles and Data*, 4th edn. Pitman, London, 1952 (for the Council of the Royal Aeronautical Society).

APPENDIX: CALCULATION OF STRAINS AT EDGE OF WEB CUTOUT

Agarwal and Broutman[30] considered an infinite orthotropic plate with a hole of radius R subjected to a uniform stress, σ, parallel to the y axis at infinity as shown in Fig. A1. If the axes are assumed normal to the planes of elastic symmetry, the normal stress, σ_y, along the x axis in front of the hole is given, approximately, by:

$$\sigma_y(x,0) = \frac{\sigma}{2}\left\{2 + \left(\frac{R}{x}\right)^2 + 3\left(\frac{R}{x}\right)^4 - (k_T - 3)\left[5\left(\frac{R}{x}\right)^6 - 7\left(\frac{R}{x}\right)^8\right]\right\} \quad \text{(A1)}$$

where k_T is the orthotropic stress concentration factor for an infinite-width plate and can be determined from the following relationship:

$$k_T = 1 + \sqrt{\frac{2}{A_{22}}\left(\sqrt{A_{11}A_{22}} - A_{12} + \frac{A_{11}A_{22} - A_{12}^2}{2A_{66}}\right)} \quad \text{(A2)}$$

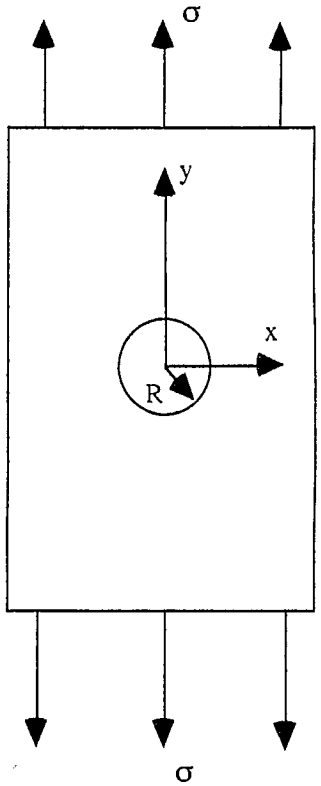

Fig. A1. Plate containing circular hole of radius R under the influence of a remote stress, σ.

where A_{ij} are the in-plane laminate stiffnesses as determined from laminated plate theory and the material data of Table 1. For the carbon/epoxy and glass/epoxy beams, k_T is calculated to be 4·41 and 3·60, respectively. The radius of the large cutouts in both the carbon and glass I-beams is nominally 30 mm.

Because the strain gauges have a finite area, the strain values are not point values. Consequently, experimentally measured tensile strains around the cutouts in the carbon and glass beams, some 1·0 and 1·4%, respectively, correspond to a distance of 2–3 mm from ahead of the cutouts. These strains in turn correspond to strains of 1·4–1·6% at the edge of the cutout in the carbon/epoxy beam and 1·8–2·0% at the edge of the cutout in the glass/epoxy beam.